Elastic properties of superconducting Chevrel-phase compounds

B. Wolf, J. Molter, G. Bruls, and B. Lüthi
Physikalisches Institut der Universität Frankfurt, D-60054 Frankfurt, Germany

L. Jansen
High Magnetic Field Laboratory, F-38042 Grenoble, France

(Received 28 September 1995; revised manuscript received 31 January 1996)

We present elastic constant and magnetic data for the two Chevrel-phase compounds $PbMo_6S_8$ and $Eu_{0.6}Sn_{0.4}Mo_6S_8Br_{0.1}$. A strong softening in the elastic constants as a function of temperature is observed for the longitudinal and transverse modes in both compounds in the normal state. This effect can be explained with a deformation potential coupling. We find no structural transition in the temperature range 1.2–300 K. In the superconducting regime the attenuation and sound velocity exhibit pronounced anomalies which can be explained using the so-called thermally assisted flux flow model. These data together with electrical resistivity measurements enable us to construct a detailed B-T phase diagram.
[S0163-1829(96)04526-2]

I. INTRODUCTION

Since the discovery of a new series of ternary molybdenum sulfides in 1971 by Chevrel *et al.*,[1] their unusual superconducting properties have generated a large number of different investigations in these compounds. Especially the extremely enhanced critical fields are interesting for technical applications. Another interesting aspect in these compounds is the coexistence of magnetic order and superconductivity and the reentrant superconducting transitions found in some of these systems.[2] Chevrel phases have the general chemical formula $M_xMo_6S_8$, where M stands for a large number of metals. The superconducting properties are mainly determined by the band structure of the Mo_6S_8 cluster, whereas the magnetic behavior depends on the metal atoms M.

In this paper we investigate polycrystalline sintered samples of $PbMo_6S_8$ and $Eu_{0.6}Sn_{0.4}Mo_6S_8Br_{0.1}$ with ultrasonic techniques for temperatures between 300 and 1.2 K and magnetic fields up to 30 T. We performed these measurements to obtain detailed information on the electron-phonon interaction in the normal state, the B-T phase diagram, and the vortex dynamics in the superconducting regime for different Chevrel compounds. This work is part of a larger program investigating various superconducting materials such as heavy fermion systems, mixed valence, etc. (Ref. 3 and references therein), using ultrasonic techniques. The samples were also characterized by resistivity- and ac-susceptibility measurements.

The experimental setup is briefly described in Sec. II. In Sec. III we show elastic constant measurements and discuss the elastic behavior of the samples in the paramagnetic region especially the strong softening effects using a deformation potential coupling. The superconducting properties are treated in Sec. IV. The pronounced elastic anomalies in magnetic fields can be described quantitatively with the thermally assisted flux flow (TAFF) model, which is explained in Sec. V.

II. EXPERIMENT

The samples were given to us by W. Goldacker from the Forschungszentrum Karlsruhe ($PbMo_6S_8$) and Ø. Fischer from the University of Geneva ($Eu_{0.6}Sn_{0.4}Mo_6S_8Br_{0.1}$). The acoustic measurements were performed with a setup described in Ref. 3. The high-field experiments up to 30 T were performed at the MPI-SNCI high-field facilities in Grenoble. The ac susceptibility was determined with a pickup coil system and a mutual inductance bridge operating at a frequency of 120 Hz. The resistivity data were taken with a standard four-lead technique. The Debye temperature was determined from the elastic constant measurements (see Table I) using Ref. 4. From the x-ray and measured density (see Table I), we obtain a filling factor for our samples of 75% ($Eu_{0.6}Sn_{0.4}Mo_6S_8Br_{0.1}$) and 93% ($PbMo_6S_8$).

III. PARAMAGNETIC REGION

In the paramagnetic region the elastic constants for both $PbMo_6S_8$ and $Eu_{0.6}Sn_{0.4}Mo_6S_8Br_{0.1}$ exhibit strong softening effects for longitudinal-and transverse modes from room temperature down to the superconducting transition temperature T_c as seen in Figs. 1(a), (b) and 2(a), (b). The relative changes in this temperature range are about 10% and 20% for longitudinal and transverse modes in both compounds. These softening effects are rather similar to these of the A-15 compounds, although somewhat smaller.[5] The inset in each figure shows the temperature dependence of the elastic constants near T_c.

We can interpret these softening effects with a deformation potential analysis, used widely for semiconductors[6] and metals.[7–9] In this mechanism electrons redistribute between strain-shifted energy pockets which are located at equivalent k points of the Brillouin zone. In order that this mechanism give an observable temperature dependence, one needs $\Delta E = E_F - E_0 \approx 100$ K. Here E_F is the Fermi energy and E_0 is the bottom of the conduction electron band. In addition, the electronic density of states $N(E)$ and the deformation

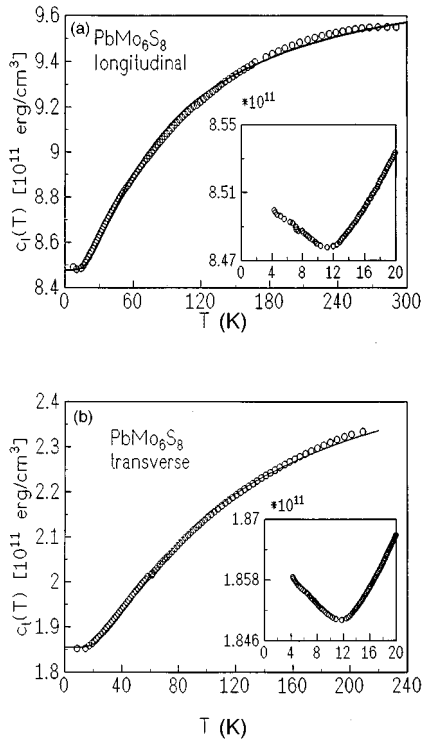

FIG. 1. Temperature dependence of the elastic constants of $PbMo_6S_8$. The inset gives the detailed behavior near T_c. (a) Longitudinal mode, (b) transverse mode. The solid lines are calculations based on the deformation potential coupling (see text). The x-ray density was used to determine the elastic constants.

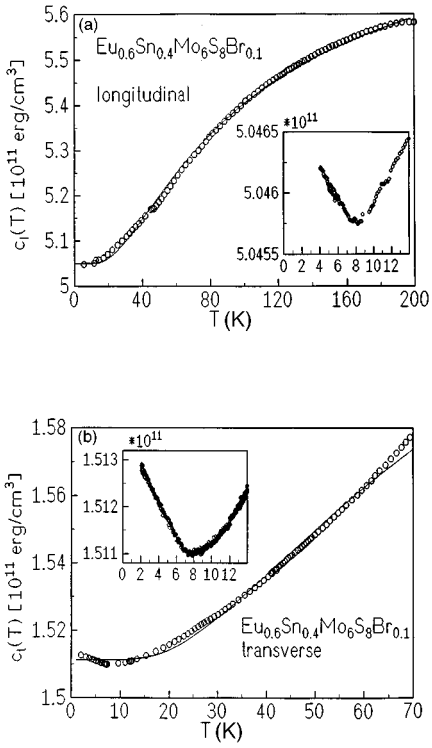

FIG. 2. Temperature dependence of the elastic constants of $Eu_{0.6}Sn_{0.4}Mo_6S_8Br_{0.1}$. The inset gives the detailed behavior near T_c. (a) Longitudinal mode, (b) transverse mode. The solid lines are calculations based on the deformation potential coupling (see text). The x-ray density was used to determine the elastic constants.

potential coupling constant d have to be large. One gets[9]

$$c = c_0 - 2d^2N\left[1 - \exp\left(-\frac{\Delta E}{kT}\right)\right]. \tag{1}$$

A fit to the elastic constants in Figs. 1(a), (b) and 2(a), (b) is shown by the solid lines. The parameters ΔE and d^2N are listed in Table I for the two compounds. The background elastic constants were taken as constant for the temperature region investigated. The coupling constants for the two substances are rather similar, with the longitudinal one 2–4 times larger than the transverse one (see Table I).

The large value of $N(E)$ is substantiated by band structure calculations for $PbMo_6S_8$ revealing a large density of states peak in the vicinity of the Fermi energy[10] originating mainly from the Mo $4d$ band. Taking $N(E_F)=0.67$/eV spin $=8.43\times10^{33}$ (erg cm)$^{-1}$, we get for the longitudinal coupling constant $|d|=2.1\times10^4$ K. Expressing this deformation potential constant as a Grüneisen parameter Ω,[9] we get $|\Omega|=d/\Delta E=296$, a rather large value for a Chevrel phase material.

In the samples we investigated there is no sign of a structural phase transition which was inferred from x-ray measurements in $PbMo_6S_8$.[11] We examined especially the temperature region around 140 K where the onset of this transition should take place. Since elastic constants are a highly sensitive probe for structural phase transitions,[5] we should have observed this transition. A possible explanation lies in the oxygen concentration of the samples which suppresses this structural transition.[12]

We also investigated the magnetic field dependence of the elastic constants in the normal-state region by taking the spin splitting of the conduction band into account (analogous to the Pauli spin paramagnetism in finite fields). Equation (1) is generalized to

$$\begin{aligned} c(T,B) = c_0 - 2Nd^2\Bigg(1 - e^{-2\Delta E/k_BT}\left[1 - \cosh^2\left(\frac{g\mu B}{k_BT}\right)\right] \\ - e^{-\Delta E/k_BT}\cosh\left(\frac{g\mu B}{k_BT}\right) \\ \times\left\{1 - e^{-2\Delta E/k_BT}\left[1 - \cosh^2\left(\frac{g\mu B}{k_BT}\right)\right]\right\}^{1/2}\Bigg). \end{aligned} \tag{2}$$

In the field and temperature ranges of 0–14 T and 10–30 K, the magnetic field effect on the elastic constants according to Eq. (2) is rather small, the relative change in the elastic constant being of the order of 10^{-3} for $B=10$ T and $T=20$ K. Experimentally, we observe a small field effect (Fig. 3) for the normal-state region. The effect is largest in the temperature range 15–35 K and of the order of $+3\times10^{-4}$, which is nearly the same order of magnitude as the calculated one. Since the measurements of Fig. 3 are taken for longitudinal modes with the k vector parallel to the magnetic field, no Lorentz force effect is present in this configuration. At the moment we have no explanation for the field dependence in the superconducting state in the vicinity of T_c. The relative change at 9 K in the vicinity of T_c is -8×10^{-4} between 0 and 14 T.

TABLE I. Physical parameters of $PbMo_6S_8$ and $Eu_{0.6}Sn_{0.4}Mo_6S_8Br_{0.1}$ in the normal and superconducting states.

	$PbMo_6S_8$	$Eu_{0.6}Sn_{0.4}Mo_6S_8Br_{0.1}$
X-ray density (g/cm^3)	6.20	5.80
Density (g/cm^3)	5.75	4.30
Elastic constants (100 K)		
Longitudinal (10^{11} erg/cm^3)	9.12	5.40
Transverse	2.14	1.61
Coupling constants d^2N (10^{11} erg/cm^3)		
Longitudinal	0.705	0.418
Transverse	0.370	0.105
ΔE (K)		
Longitudinal	71	86
Transverse	91	85
Debye temperature (K)	245	203
Transition T_c (K)	13,2	7,8

IV. SUPERCONDUCTING PHASE TRANSITION REGION

Of particular interest is the region of the superconducting transition. In Figs. 4(a) and 4(b) we show electrical resistivity measurements together with an enlarged view of sound velocity measurements for the two compounds taken from Figs. 1(a), 1(b) and 2(a), 2(b). It is seen that at the temperature where the resistivity drops down we also observe an anomaly in the elastic constants. Theory predicts a steplike change of the order of $-g^2/\beta$ where β is the fourth-order Landau parameter and g the strain-order parameter coupling constant.[13] This steplike change is not seen in Figs. 4(a), 4(b) for both the Pb and Eu compounds and for the longitudinal and transverse modes. For BCS and heavy fermion superconductors, the relative steplike change is of the order of 10^{-4}. The reason why this steplike change is not observed in Figs. 4(a), 4(b) is not clear. It could be due to the sintered materials used here. Instead of a steplike change, we observe a rather broad minimum at or just below T_c, which was determined from ac-susceptibility (not shown) and resistivity measurements.

Figures 5(a), 5(b) show the electrical dc resistivity as a function of temperature in different magnetic fields for both compounds. In $Eu_{0.6}Sn_{0.4}Mo_6S_8Br_{0.1}$ the onset of the sharp superconducting transition is slightly above 8 K with a width of the transition of 0.40 K. In $PbMo_6S_8$, T_c is around 13.2 K. The resistivity and ac-susceptibility measurements [not shown in Figs. 5(a), 5(b)] give about the same T_c. These measurements are used to construct the B_{c2} curve for a B-T phase diagram (see Fig. 6). The jumps in $\rho(T,B)$ characterize the $B_{c2}(T)$ curve. The other lines shown in Fig. 6 are discussed below.

V. DISCUSSION OF THE TAFF MODEL FOR CHEVREL PHASES

In both compounds there are large magnetoacoustic effects observed in the superconducting phase for the transverse mode with the orientation $B \| k$ between the wave vector k and the external magnetic field B. Below T_c there are positive steplike changes in the elastic constants combined with large attenuation peaks for high magnetic fields shown for $Eu_{0.6}Sn_{0.4}Mo_6S_8Br_{0.1}$ [Figs. 7(a), 7(b)]. The step height is a function of a magnetic field.

We describe these magnetoacoustic anomalies in the superconducting state with the TAFF model (thermally assisted flux flow) proposed by Anderson and Kim.[14] This model is usually used for the description of the penetration of magnetic flux into a type-II superconductor and the temperature dependence of the critical current. One assumption of this model is a strong pinning of the vortices in the sample. The system should be an extreme type-II superconductor because the pinning energy U is proportional to the square of the thermodynamic critical field B_c^2 and to the third power of the coherence length ξ^3. Because of the short coherence length in Chevrel phases, there is only a local pinning of vortices at point defects. So one obtains a distribution of the vortices in the form of flux-line bundles for temperatures near T_c.

The presence of a lattice of strongly pinned vortices gives rise to a stiffening of the elastic modes in this temperature region as observed [see Fig. 7(b)]. The sound velocity and ultrasonic attenuation can be used to study the dynamical properties of a flux-line lattice (FLL). The coupling between the FLL and the sound wave mediated through the pinning

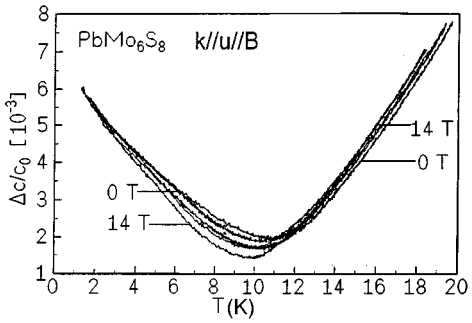

FIG. 3. Magnetic field dependence of the longitudinal sound velocity in the temperature range 0–20 K for $PbMo_6S_8$.

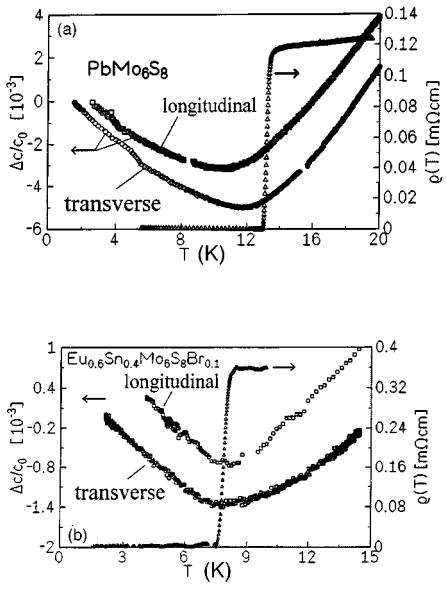

FIG. 4. Resistivity and relative sound velocity change near the superconducting phase transition. (a) $PbMo_6S_8$, (b) $Eu_{0.6}Sn_{0.4}Mo_6S_8Br_{0.1}$.

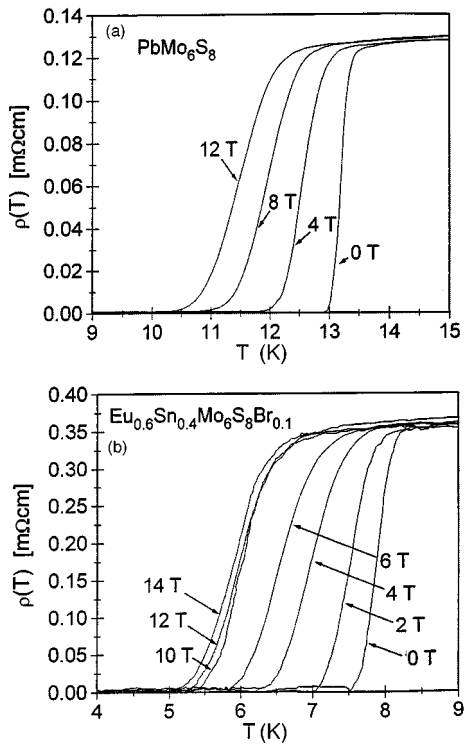

FIG. 5. Electrical resistivity as a function of temperature and magnetic field (a) $PbMo_6S_8$, (b) $Eu_{0.6}Sn_{0.4}Mo_6S_8Br_{0.1}$.

strongly modifies the sound velocity and attenuation. Ultrasound experiments really test the bulk properties of granular samples and are less sensitive to surface and grain boundary effects in comparison with resistivity measurements. So they are very suitable for an investigation of the vortex dynamics in Chevrel phases.

Now we describe the change of the elastic constant and the ultrasound attenuation in the TAFF model. After a small distortion, the FLL will relax to equilibrium. In our experiments we use transverse sound waves with $B \| k$ and $B \perp u$, where u is the displacement. We must combine the elastic properties of the crystal lattice and the FLL. This was done in Ref. 15, and one obtains the following equations for the

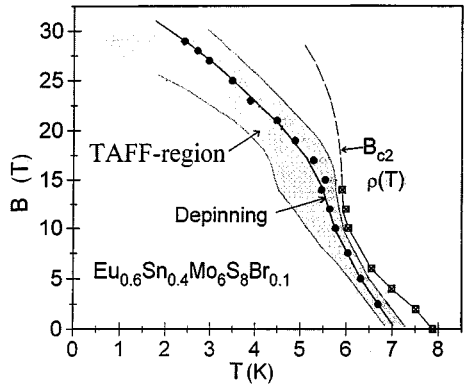

FIG. 6. B-T phase diagram for $Eu_{0.6}Sn_{0.4}Mo_6S_8Br_{0.1}$ as determined from resistivity (open squares), sound velocity, and ultrasound attenuation measurements. The solid circles are determined from the attenuation maximum. The width of the ultrasound anomalies characterizes the TAFF region.

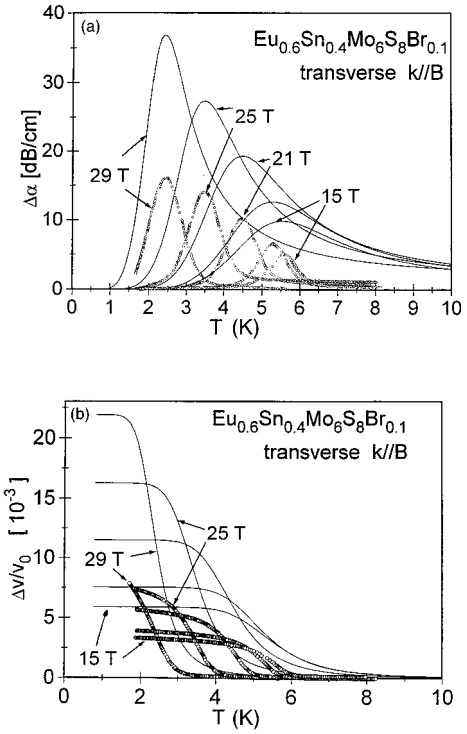

FIG. 7. (a) Ultrasonic attenuation (b) Sound velocity. Both measurements as a function of temperature in magnetic fields for $Eu_{0.6}Sn_{0.4}Mo_6S_8Br_{0.1}$ at low temperatures. The solid lines are calculations based on the TAFF model. A possible filling factor correction is neglected. The fields used are 15, 17, 21, 25, and 29 T.

relative shift in the sound velocity and ultrasound attenuation:

$$\frac{\Delta v_t}{v_t} = \frac{1}{2\rho_m c v_t^2} \frac{c_{44}\omega^2}{\omega^2 + (c_{44}\Gamma k^2)^2},$$
$$\Delta\alpha = \frac{20\ln(e)\omega^2}{2\rho_m v^3} \cdot \frac{c_{44}^2 \Gamma k^2}{\omega^2 + (c_{44}\Gamma k^2)^2}. \tag{3}$$

Here v_t is the transverse sound velocity, α the attenuation, c_{44} the vortex elastic constant ($c_{44} = B^2/4\pi$), ρ_m the mass density, $\omega/2\pi$ the frequency, and k the wave vector of the sound wave. The background damping is ignored in these expressions. Γ is a diffusion coefficient which is correlated to the dc resistivity $\rho = (4\pi/c^2)c_{44}\Gamma$.

In the TAFF model the resistivity ρ in the region where there is a thermally assisted hopping of flux-line bundles is given by[16]

$$\rho = \rho_{\mathrm{TAFF}} \exp\left[-\frac{U(B)}{kT}\right], \tag{4}$$

with ρ_{TAFF} constant in this regime. Combining Eqs. (3) and (4), one finds, for the temperature T^* of the attenuation peak which is associated with a step in the sound velocity, $T^* = U(B)/\ln[c^2\ \rho_{\mathrm{TAFF}} k^2/4\pi\omega]$.

Figure 7(a) exhibits the ultrasound attenuation as a function of temperature for fields up to 30 T. In the normal state there is only a small temperature-independent attenuation. Below T_c the attenuation starts to increase until a maximum is reached. The position of this maximum characterizes the

depinning line in the B-T phase diagram shown in Fig. 6. For $T \rightarrow 0$ K the ultrasound attenuation decreases. Above the depinning line there is a thermally assisted hopping of flux-line bundles, whereas for low temperatures and small magnetic fields all vortices are rigidly pinned. There is no hysteresis as a function of temperature. As mentioned before, the maximum in the ultrasound attenuation is accompanied by a steplike anomaly in the elastic constant. Figure 7(b) shows measurements from l5 to 29 T. The steplike anomaly starts to increase for fields around 5 T and becomes very large for 30 T. Here the change in the sound velocity is nearly 1% for 10 MHz. Results similar to the ones shown in Figs. 7(a), (b) have been obtained for high-T_c materials by vibrating-reed techniques.[17]

For the calculated fit we used the following parameters: $v_t = 2.76 \times 10^3$ m/s, sound wave frequency 10 MHz, and $\rho_{\mathrm{TAFF}} = 0.35$ mΩ cm. Equation (3) gives only a semiquantitative description of the experimental results as seen in Figs. 7(a), (b), however. The discrepancy could partly be due to the filling factor of our granular samples, cited in Sec. II (see Ref. 15).

In Fig. 6 we show the B-T phase diagram of $Eu_{0.6}Sn_{0.4}Mo_6S_8Br_{0.1}$ constructed from the dc-resistivity and ultrasound measurements. The B_{c2} curve is determined by the resistance measurements as discussed above. The positive curvature of B_{c2} is very typical for the Sn-doped Eu compound.[18] For high Sn concentrations this anomalous behavior is due to the Jaccarino-Peter effect.[19] Therefore, our anomalous behavior could be due to such a precursor effect. The depinning line shown in Fig. 6 is below the B_{c2} curve, an effect already observed in high-temperature superconductors.[20]

The ultrasound measurements together with the dc-resistivity values yield the activation energies for the thermally assisted hopping in both compounds as a function of magnetic field. For $Eu_{0.6}Sn_{0.4}Mo_6S_8Br_{0.1}$ this energy is around 25 K at 5 T and decreases to 11 K at 30 T. With 32 K at 5 T, these values are somewhat larger in $PbMo_6S_8$.

In conclusion, as shown in Table I and the figures, our investigation provides a number of important physical parameters such as the deformation potential coupling constant, elastic constant, and vortex bundle activation energies. In addition, the superconducting phase diagram with the vortex depinning region was obtained.

ACKNOWLEDGMENTS

We would like to thank Professor Ø. Fischer, Geneva, and Dr. W. Goldacker, Karlsruhe, for providing us the sample used in this investigation. We wish to thank Dr. M. Decroux for critical comments about the manuscript. This research was supported by the Deutsche Forschungsgemeinschaft DFG, Sonderforschungsbereich 252.

[1] R. Chevrel, M. Sergent, and J. Prigent, J. Solid State Chem. **3**, 515 (1971).
[2] Ø. Fischer, Appl. Phys. **16**, 1 (1978).
[3] B. Lüthi, G. Bruls, P. Thalmeier, B. Wolf, D. Finsterbusch, and I. Kouroudis, J. Low Temp. Phys. **95**, 257 (1994).
[4] O. L. Andersen, J. Phys. Chem. Solids. **24**, 909 (1963).
[5] L. R. Testardi, in *Physical Acoustics*, Vol. X, edited by W. P. Mason and R. N. Thurston (Academic, New York, 1973), B. Lüthi and W. Rehwald, in *Structural Phase Transitions I*, edited by K. A. Müller and H. Thomas, Topics in Current Physics (Springer, New York, 1981).
[6] R. W. Keyes, *Solid State Physics*, edited by F. Seitz and D. Turnbull (Academic, New York, 1967).
[7] M. Niksch, B. Lüthi, and J. Kübler, Z. Phys. B **68**, 291 (1987).
[8] T. S. Kwon, J. C. Park, K, Nahm, H. S. Noh, and C. K. Kim, Phys. Rev. B **49**, 4388 (1994).
[9] P. Thalmeier and B. Lüthi, in *Handbook on the Physics and Chemistry of Rare Earths*, edited by K. A. Gschneidner, Jr. and L. Eyring (North-Holland, Amsterdam, 1991), Vol. 14.
[10] O. K. Anderson, W. Klose, and H. Nohl, Phys. Rev. B **17**, 1209 (1978).
[11] M. François, K. Yvon, D. Cattani, M. Decroux, R. Chevrel, M. Sergent, S. Boudjada, and Th. Wroblewski, J. Appl. Phys. **75**, 423 (1994).
[12] M. Decroux (private communication). The small anomalies seen in $Eu_{0.6}Sn_{0.4}Mo_6S_8Br_{0.1}$ at 42 K in both modes do not exhibit an effect in the ultrasound attenuation. Therefore, we refrain from interpreting these very small anomalies.
[13] P. Thalmeier, B. Wolf, D. Weber, G. Bruls, B. Lüthi, and A. A. Menovsky, Physica C **175**, 61 (1991).
[14] P. W. Anderson and Y. B. Kim, Rev. Mod. Phys. **36**, 39 (l964); P. W. Anderson, Phys. Rev. Lett. **9**, 309 (l962).
[15] J. Pankert, Physica C **168**, 335 (l990); P. Lemmens, Ph.D. thesis, RWHT, Aachen, 1992.
[16] E. H. Brandt, Physica C **185**, 270 (1992).
[17] Z. Xu, L. E. de Long, J. W. Brill, J. Hou, H. Drulis, Y. Zheng, D. G. Hinks, M. L. Norton, H. Tang, and C. P. Brock, J. Supercond. **7**, 835 (1994); A. Gupta, P. Esquinazi, and H. F. Braun, Phys. Rev. Lett **63**, 1869 (1989).
[18] O. Peña and M. Sergent, Prog. Solid State Chem. **19**, 165 (1989).
[19] V. Jaccarino and M. Peter, Phys. Rev. Lett. **9**, 290 (1962).
[20] P. Lemmens, P. Fröning, S. Ewert, J. Pankert, G. Marbach, and A. Comberg, Physica C **174**, 289 (1991).